Journal of Sound and Vibration 327 (2009) 354–367

Contents lists available at ScienceDirect

Journal of Sound and Vibration

journal homepage: www.elsevier.com/locate/jsvi

Measurement and inverse estimation of 3D anisotropic flow resistivity for porous materials

Peter Göransson *, Rémi Guastavino [1], Nils-Erik Hörlin

Marcus Wallenberg Laboratory for Sound and Vibration Research, KTH Aeronautical and Vehicle Engineering, SE-100 44 Stockholm, Sweden

ARTICLE INFO

Article history:
Received 25 February 2009
Received in revised form
24 June 2009
Accepted 29 June 2009
Handling Editor: Y. Auregan
Available online 14 August 2009

ABSTRACT

This paper presents a new methodology for estimating the anisotropic flow resistivity for porous materials. From pressure measurements on a cubic or parallelepiped sample of a porous material, the flow resistivities are determined using inverse estimation. The core of the estimation is a series of 3D solutions to Darcy's law, where the flow resistivity tensor is varied until the sum of the quadratic errors between measured and computed pressures is minimised. The overall approach and experimental set-up used, enabling efficient measurements of high quality, are described in some detail together with the main steps of the measurement and estimation procedures. Results from a fibrous glass wool and a polyurethane foam are discussed and compared to standard measurement data.

1. Introduction

Traditionally porous materials used in vibro-acoustic applications have been treated as isotropic in terms of the elastic as well as the acoustic properties. However, it is well known that, due to the manufacturing processes involved, there is a certain degree of anisotropy in all porous materials, be it foamed polymers, fibrous wool, etc. For fibrous wool, the degree of anisotropy, with respect to the flow resistivity, is mostly low and linked to the layering of the fibres and the subsequent compression to desired thickness and density. Commonly they are considered to be transversely isotropic. For foamed materials, the anisotropy is related to the influence of gravity during expansion in combination with the placement of the injection nozzles, depending on the manufacturing method used. For these materials the degree of anisotropy is higher.

Standard measurement techniques usually allow for at most identification of the body coordinate directions of a material. This is achieved through an extraction of samples and subsequent testing of these in unidirectional conditions. As the full degree of anisotropy is in general unknown, this is a rather delicate step. Thus, there is a need for a method to identify the full anisotropic properties of a porous material without any imposed assumptions on symmetry in the properties of the material and preferably without extensive sample preparation.

The current paper proposes a methodology, which alleviates the restricting assumptions on isotropy, using a non-destructive testing approach which allows for the identification of the anisotropic flow resistivity tensor. The underlying assumption throughout this paper is that Darcy's law [1] governs the static fluid flow in the porous medium, i.e. neglecting viscosity and inertial effects in the flow. This is justified by the intended modelling context in which the estimated flow

* Corresponding author. Tel.: +46 8 7907963.
E-mail address: pege@kth.se (P. Göransson).
[1] Now at Bruel & Kjaer, Denmark.

0022-460X/$ - see front matter © 2009 Elsevier Ltd. All rights reserved.
doi:10.1016/j.jsv.2009.06.028

resistivity will be used, i.e. linear acoustic wave propagation in the frame of Biot models [2]. It thus should be seen as a natural extension of the standard isotropic Biot–Johnson–Allard models [2–4].

Whereas in acoustics, porous materials have traditionally been, and for most practical purposes still are, regarded as isotropic in terms of both acoustic and elastic properties, several authors have quite recently discussed different models of an assumed non-isotropic material [5–7]. As mentioned above, most of these models have been regarded as transversely isotropic, a valid assumption for fibrous wool but possibly too restrictive for foamed polymers.

In other fields where porous media are encountered, and there is an interest in modelling their behaviour under some specific flow or load conditions, the notion of an anisotropic flow resistivity, or rather its inverse permeability, tensor is well established. For dolomite, a rock reservoir, Sharma gave the normalised, full anisotropic permeability tensor [8]. For cancellous bone Kohles et al. [9], presents anisotropic permeability results from static flow measurements on extracted samples.

The principal approach taken, i.e. identifying the full, anisotropic flow resistivity tensor is to the knowledge of the authors original. Whereas measurements on anisotropic glass fibre wool have been published recently, see Refs. [6,7,10], these have been performed on extracted directional samples, and thus have been limited to determining the flow resistivities along these directions, i.e. the diagonal terms of the tensor in a body coordinate system aligned with the sample surfaces. It is interesting to note that a similar cubic sample arrangement was used by Kohles et al. [9], however also in there only the flow resistivities in the body coordinate system aligned with the sample boundaries were reported. Thus, a method allowing for the estimation of the full flow resistivity tensor matrix, in particular the cross coupling terms between the measured flow directions, seems to be of interest for several engineering fields.

The paper begins with a review of the experimental set up, including definitions of faces of the test specimen, and the important aspect of sample preparation. This is then followed by a discussion of the model used to simulate the anisotropic flow resistivity, including the inverse estimation approach proposed. The methodology is applied to two different types of porous materials, one glass fibre wool and one polyurethane foam, for which the flow resistivity tensor is estimated and the principal directions are computed. The paper concludes with a sensitivity analysis where the influence of variations in the input data is illustrated for the two materials.

2. Approach

The aim of the current paper is to discuss a novel approach to the determination of the flow resistivities of a porous material. It is based on a precise measurement set up, which is a generalisation of the standardised static flow-pressure drop measurement [6,11,12]. Whereas the standard set up requires cylindrical samples to be extracted for each direction of interest, the novel equipment proposed here, utilises a single (cubic) sample and is inherently non-destructive in the sense that the same sample may be used for determining other properties such as e.g. elasticity. To identify the flow resistivities, a series of tests are conducted on cubic specimens, cut out from a block, in X-, Y- and Z-flow conditions (X–Y–Z being the body coordinate system defined such that X is in the vertical direction and Y, Z are in the horizontal plane) using the configuration shown in Fig. 1. These data, i.e., differential pressure and static flow velocity, are then fed into an inverse estimation procedure, where a series of 3D solutions to Darcy's law [1] are computed for a given symmetric, flow resistivity tensor which is varied until the quadratic error between measured and computed pressures reaches a minimum. The corresponding values are then interpreted as the static flow resistivities for the tested material sample.

The paper is structured in three main parts, first the experimental set up is reviewed, then the inverse estimation procedure is formulated and finally results for both a fibrous wool and a polymer foam are discussed.

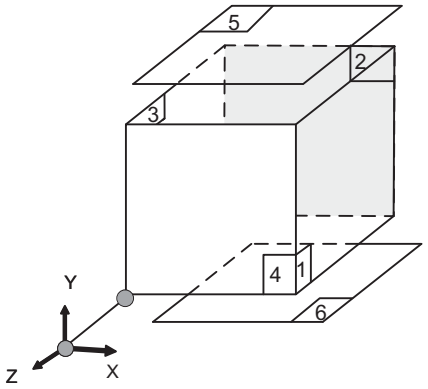

Fig. 1. Cube with side L and face definitions: face 1 (resp. 3) at the plane $x = L$ (resp. $x = 0$), face 2 (resp. 4) at the plane $z = -L$ (resp. $z = 0$) and face 5 (resp. 6) at the plane $y = L$ (resp. $y = 0$).

3. Experimental arrangement

3.1. Set up

The symmetric cubic set up developed and used to measure the pressure drop in different directions, has the following main features, see Fig. 2 for an graphical representation of the different parts:

- A cubic box built out of 5 mm aluminium plates, having sides with 99 mm inner length dimension and openings of 42 mm diameter at all of its faces, allowing for a fast recording of the pressure differences of a parallelepiped sample.
- The openings are sealed by plugs which are individually removable.
- For each measurement one of the openings is connected through an airtight adapter to a constant flow device, and the other five are then, one at a time, set at atmospheric pressure by removing the particular plug.
- The flow velocity is measured simultaneously with the pressure at the in-flow hole, when the different faces are open and closed respectively.

The prepared sample labelled D in Fig. 2 (all capitalised labels of the following paragraph refer to Fig. 2), is placed and clamped between the two parts labelled C, which are joined together with screws. In case of materials that are difficult to cut precisely (like fibrous wool) a sheet of silicone or any soft closed cell material is placed between the sample and the interior walls of the box in order to prevent air gaps. For the measurements to produce high quality results, it is important that the sample is slightly compressed in order to prevent air to travel along the walls. The upper and lower plates (labelled A) are then placed at the top and the bottom of the sample and screwed to C. The sample is now trapped in a cube with one opening on every face; each opening can be closed with a plug (labelled B) or connected to a pipe with a flow. The flow may be directed from one opening on one face to any of the opening on another face by inserting or removing the plugs allowing for a recording of the corresponding pressures and velocities, see Fig. 3.

A pressure sensor SwemaMan 80 is used to estimate the flow rate passing through a laminar element Meriam 50MJ10-12 just before it enters into the sample; the actual pressure drop over the tested flow directions of the sample is estimated using a differential pressure transmitter from Furness controls model FCO332, see Fig. 4.

For each inflow face five data sets, i.e. the inward flow and corresponding pressure drop along the sample, are recorded. Whereas for each sample there are 30 pairs of data (six faces with inflow and for each of these five faces of outflow), only 15 of them are used because of the symmetry of the measurement and the assumed reciprocity of the flow resistivity tensor, as discussed below. The remaining measured data are used as quality control checks, a measurement is not accepted if the deviation is larger than 5 percent between reciprocal directions. In this context, it is worth mentioning that, the

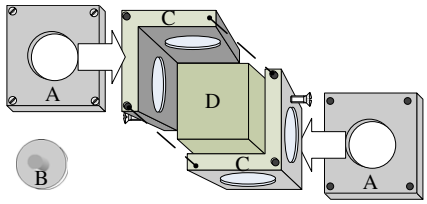

Fig. 2. Mounting device for cubic samples.

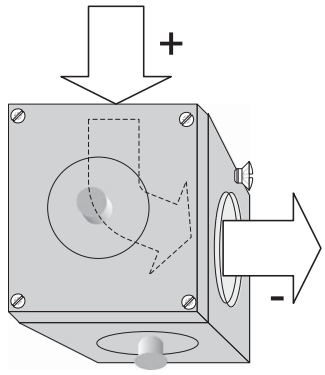

Fig. 3. Measurement principle for the proposed method.

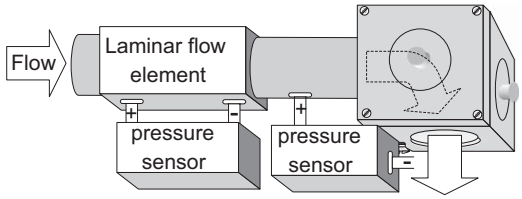

Fig. 4. General arrangement of flow and pressure sensors in the proposed set-up.

repeatability of the set up is quite satisfactory. After dismounting and remounting a sample in the holding device discussed above, a variation of a maximum of 7 percent in the measured differential pressure was observed.

A limiting factor concerning the quality of the proposed measurement method is related to the surface of the porous material and the sealing against the sides of the cube. To ensure a reproducible measurement, the block sample is cut slightly larger, ≈ 3 mm along each edge.

Each sample is tested at different flow rates to insure that the fluid velocity is low enough i.e. to ensure linearity. The flow velocities finally used for the test results used in the estimation discussed here, were of the order of 5 mm/s, although higher than the recommended ISO flow rate [11], still found to be providing a linear relation between in-flow velocity and pressure differential.

3.2. Sample preparation and measurement quality

The major difficulty, and perhaps the most severe limitation of the present method, also shared by the standard measurement method for flow resistivity, lies in the preparation of the samples themselves. Initially, 100 mm width cubic shaped samples were cut and later re-cut with a sharp blade to come as close as possible to a cubic shape. In this process it was noted that mechanical cutting tends to deform the sample locally as soon as the blade is applied. This had as a result that the edges were not straight after cutting. Being more pronounced for polymer foams than fibrous wool, this aspect was monitored in terms of the quality of the measurements performed using the set up proposed here. For each sample the symmetry of the measured, expectedly reciprocal, pressure differences and flow velocities as discussed above were carefully checked.

4. Inverse estimation

4.1. Governing equations

As the purpose of the particular aspects of material characterisation discussed here, is to determine properties useful in linear acoustic wave propagation in the frame of Biot models [2], the fluid flow inside the porous domain is assumed to be governed by Darcy's law [1]. Thus, it is determined by the second-order permeability tensor $\boldsymbol{\kappa}$, the dynamic viscosity η, the pressure p and the volume average velocity $\mathbf{v} = \{v_x, v_y, v_z\}$ together with a proper set of boundary conditions.

Darcy's law states that

$$-\frac{\boldsymbol{\kappa}}{\eta}\nabla p = \mathbf{v} \tag{1}$$

which together with an assumed incompressibility condition

$$\nabla \cdot \mathbf{v} = 0 \tag{2}$$

gives

$$\nabla\left(\frac{\boldsymbol{\kappa}}{\eta}\nabla p\right) = 0 \tag{3}$$

or rewriting Eq. (3) in terms of the second-order flow resistivity tensor $\boldsymbol{\sigma}$

$$\nabla(\boldsymbol{\sigma}^{-1}\nabla p) = 0 \tag{4}$$

with boundary conditions

$$\nabla p \cdot \mathbf{n}_i = \bar{\sigma}\bar{\mathbf{v}} \cdot \mathbf{n}_i, \quad \mathbf{x} \in \mathbf{X}_i^{\text{in-flow}}, \ i = 1, \ldots, 6 \tag{5}$$

$$\nabla p \cdot \mathbf{n} = 0, \quad \mathbf{x} \in \mathbf{X}^{\text{rigid walls}} \tag{6}$$

$$p = 0, \quad \mathbf{x} \in \mathbf{X}_j^{\text{out-flow}}, \quad j = 1, \ldots, 6, \quad i \neq j \tag{7}$$

where indices i and j refer to the faces of the cubic sample with definitions as given in Fig. 1, $\mathbf{x} = \{\mathbf{x}, \mathbf{y}, \mathbf{z}\}$ being the location vector, $\mathbf{X}^{\text{in-flow}}$ and $\mathbf{X}^{\text{out-flow}}$ are the inflow and outflow boundaries respectively, $\mathbf{n}$ is the normal vector pointing outwards from the domain, $\bar{\mathbf{v}}$ is the prescribed in-flow velocity at an open boundary and $\bar{\sigma}$ is an artificial isotropic flow resistivity introduced for modelling reasons as discussed in Section 4.3.

4.2. Properties of the flow resistivity tensor

In order to identify the anisotropic flow resistivity of a porous sample, some properties of the corresponding tensor have to be stated. Writing the dissipated power per volume as

$$P_{\text{diss}} = -\nabla p \cdot \mathbf{v} \tag{8}$$

observing that this is a non-negative quantity since the volume averaged, macro scale velocity $\mathbf{v}$ is from high pressure to low pressure due to the second law of thermodynamics, Wang [13].

Inserting Eq. (4), the dissipated power may be rewritten as $\mathbf{v}^T\boldsymbol{\sigma}\mathbf{v}$, which is a positive quantity if there is non-zero flow resistance in all possible directions. This is assumed to be valid here.

Then, by definition $\boldsymbol{\sigma}$ is positive definite. Furthermore, as the flow resistivity is a function of the fluid viscosity and the volume averaged velocity strain rate tensor which is symmetric, $\boldsymbol{\sigma}$ is also symmetric, Biot [14], Wang [13].

In addition, an assumption has to be made concerning the homogeneity of the flow resistivity. For a real material, there is a certain variation over space, largely attributed to the manufacturing processes involved. Here, it is assumed that this variation is small over the scale of the sample size.

4.3. Modelling

To facilitate the estimation of the flow resistivity tensor for a porous material, a numerical model of the experimental set up was developed. A critical aspect of the modelling was found to be the definition of the proper boundary conditions, in particular those related to the flow into the porous medium. In principle either the measured pressures or the known flow velocity could have been chosen to be specified and the other quantity calculated. Here the choice fell on the measured static flow velocities as input. Since the flow velocity through the cubic device is calculated from the pressure drop over the laminar flow element, an assumption concerning the flow profile was needed. Hence, in this work, it was assumed that at a certain distance away from the inlet to the cubic measurement device, the flow profiles were uniform over the cross section of the cylindrical tubes, see Fig. 4, connecting the sample holding device to the flow supply. To achieve this in the simulation, the model was fitted with tube like extensions, similar in dimensions to the actual set up used in the experiments, Fig. 5. These tubes were assigned an isotropic flow resistivity, $\bar{\sigma}$, five orders of magnitude lower than the flow resistivity in the porous medium simulated, see Eq. (5). It was verified that this approximation, introduced for defining the proper boundary conditions in terms of pressure and flow field, did not influence the results from the simulations.

Having made the choice of specifying the flow into the material as a boundary condition, the output results used from the simulations were the resulting pressure differences between the in-flow and the out-flow openings. These were readily obtained from the solution of Eq. (1) together with the boundary conditions specified in Eqs. (5)–(7), as functions of the unknown flow resistivity tensor.

For a given flow resistivity tensor, representing the porous material inside the cubic space and the tube fittings adopted, a finite element solution using the COMSOL Multiphysics package, Earth science module [15], together with the conjugate gradient solver, was calculated. For each possible flow resistivity tensor, 15 solutions of a model of the order of 20 000 degrees of freedom, using cubic order Lagrange polynomial tetrahedral elements, were computed. From these, 15 pressure differences were calculated and compared to the measured data.

To identify the different combinations of in-flow and out-flow surfaces, the notation p_{ij}^{computed} was introduced for the elements of a matrix $\mathbf{P}^{\text{computed}}$ holding the pressures computed from the solution of Eq. (1), where the indices identify the faces of the cube, according to the convention given in Fig. 1. Thus p_{34}^{computed}, should be interpreted as in-flow at face 3 (plane $x = 0$) and out-flow at face 4 (plane $z = 0$). In the theoretical model, $\mathbf{P}^{\text{computed}}$ is symmetric since a changed sign on the inlet and the outlet boundary conditions will simply reverse the flow. Note that p_{ij}^{computed} actually represents the

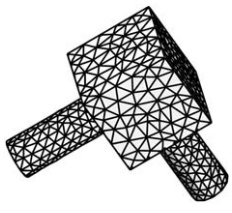

Fig. 5. Finite element mesh for cube with tube fittings, illustrated for in-flow face 2, out-flow face 3.

differential pressures between in-flow and out-flow openings of the cube, but since according to Eq. (7) the pressure at the out-flow opening is taken to be zero this is an unnecessary distinction.

4.4. Inverse estimation procedure

The flow resistivity tensor was estimated such that the sum of the square of the relative differences between the measured and the computed differential pressures was minimised, with the positive definiteness of $\boldsymbol{\sigma}$ as side condition to avoid non-admissible solution, i.e., the following optimisation problem was solved.

Find $\boldsymbol{\sigma}$ such that

$$\min \sum_{ij} \varepsilon_{ij}^2 \tag{9}$$

is minimised, where

$$\varepsilon_{ij}(\boldsymbol{\sigma}) = \left(\tfrac{1}{2}(p_{ij}^{\text{measured}} + p_{ji}^{\text{measured}}) - p_{ij}^{\text{computed}}(\boldsymbol{\sigma})\right)/p_{ij}^{\text{measured}} \tag{10}$$

subject to the positive definiteness side and boundedness conditions for the flow resistivity tensor

$$g_\upsilon(\boldsymbol{\sigma}) - 1 \le 0, \quad \upsilon = 1,\ldots,4$$

$$\sigma_{kl}^{\text{low}} \le \sigma_{kl} \le \sigma_{kl}^{\text{high}}, \quad kl = xx, xy, xz, yy, yz, zz \tag{11}$$

where

$$g_1 = \frac{\sigma_{yz}^2}{\sigma_{yy}\sigma_{zz}}, \quad g_2 = \frac{\sigma_{xz}^2}{\sigma_{xx}\sigma_{zz}}, \quad g_3 = \frac{\sigma_{xy}^2}{\sigma_{yy}\sigma_{xx}} \tag{12}$$

$$g_4 = g_1 + g_2 + g_3 - 2\frac{\sigma_{xy}\sigma_{xz}\sigma_{yz}}{\sigma_{xx}\sigma_{yy}\sigma_{zz}} \tag{13}$$

and the 15 unique combinations of in-flow and out-flow faces, see Fig. 1, were selected as

$$ij = 14, 21, 23, 24, 25, 26, 31, 34, 35, 36, 51, 54, 61, 64, 65 \tag{14}$$

In the measurement data a slight deviation from symmetry was observed for $\mathbf{P}^{\text{measured}}$. Apart from using the degree of deviation as a quality indicator, this also led to a slight modification of the object function in order to smoothen the measured data, i.e., p_{ij}^{measured} was replaced by $\frac{1}{2}(p_{ij}^{\text{measured}} + p_{ji}^{\text{measured}})$ in Eq. (10) to enforce the symmetry of $\mathbf{P}^{\text{measured}}$.

In an inverse estimation, the choice of the initial guess is crucial for the computational time required to find a minimum. Here an initial, starting flow resistivity tensor was chosen as

$$\sigma_{xx}^{\text{initial}} = p_{31}^{\text{measured}}/(LV), \quad \sigma_{xy}^{\text{initial}} = \alpha\sigma_{xx}^{\text{initial}}, \quad \sigma_{xz}^{\text{initial}} = \beta\sigma_{xx}^{\text{initial}}$$

$$\sigma_{yy}^{\text{initial}} = p_{65}^{\text{measured}}/(LV), \quad \sigma_{yz}^{\text{initial}} = \chi\sigma_{yy}^{\text{initial}}$$

$$\sigma_{zz}^{\text{initial}} = p_{24}^{\text{measured}}/(LV) \tag{15}$$

and where $0.1 < \alpha < \beta < \chi < 0.5$ were introduced in order to avoid linear dependence in the flow resistivity tensor used as the initial guess, L being the length of the sample side as defined in Fig. 1, and $V = 1$ m/s. Obviously, the value of V is far from the actual flow velocity used in the measurements. However, since the prediction model used is linear this choice was arbitrary and introduced for convenience.

In addition to the initial guesses of the actual elements of the flow resistivity tensor, also the bounds in Eq. (11) must be selected. In the current work, they were selected as

$$\sigma_{kl}^{\text{low}} = 0.05\sigma_{kl}^{\text{initial}}$$

$$\sigma_{kl}^{\text{high}} = 10\sigma_{kl}^{\text{initial}}$$

$$kl = xx, xy, xz, yy, yz, zz \tag{16}$$

The optimisation algorithm "Method of moving asymptotes" by Svanberg [16] was used to fit the model to the measured data in a least square sense, i.e. solving the problem stated by Eq. (9) using the initial starting values as given by Eq. (15). To monitor the fitness of the model, the relative pressure differences in the optimal solution, i.e. the components

Table 1
Pressure differences (Pa) measured for glass wool sample.

	Face 1	Face 2	Face 3	Face 4	Face 5	Face 6
Face 1	–	180	306	188	199	167
Face 2	181	–	231	195	174	149
Face 3	306	231	–	250	254	229
Face 4	190	197	251	–	186	164
Face 5	199	175	256	186	–	196
Face 6	168	149	230	164	196	–

corresponding to Eq. (10) were used, see the following equation:

$$\boldsymbol{\varepsilon} = \begin{bmatrix} \varepsilon_{31} & \varepsilon_{35} & \varepsilon_{34} & \varepsilon_{36} & \varepsilon_{14} \\ \varepsilon_{61} & \varepsilon_{65} & \varepsilon_{64} & \varepsilon_{51} & \varepsilon_{54} \\ \varepsilon_{21} & \varepsilon_{25} & \varepsilon_{24} & \varepsilon_{23} & \varepsilon_{26} \end{bmatrix} \tag{17}$$

Note that the indices of the matrix elements in Eq. (17), refer to the face definitions in Fig. 1.

4.5. Verification of estimation procedure

The computational parts of the proposed method were verified for a glass fibre wool with flow resistivity data provided by Tarnow [6]. Using these given elements of the flow resistivity tensor, the required pressure differences were computed for given static flow velocities and then re-used as targets in the estimation. Starting with an isotropic flow resistivity model, the correct a priori known, flow resistivities were found within 0.01 percent relative error in Eq. (17), after about 11 iterations.

5. Results

5.1. Application to fibrous glass wool

After having been verified by simulated data, the proposed method was applied to a 50 mm thick acoustic fibrous glass wool, manufactured by Ecophon (model Modus S NE nature), with mass density 29 kg/m^3. Two samples of the supplied wool were cut, in such a way that they together form a cubic sample with proper dimensions, and measured in the experimental device proposed. For convenience all measured pressures were re-scaled to unit flow velocity, i.e. 1 m/s, in line with the inverse estimation scaling. The corresponding measured pressure differences are shown in Table 1, note the high quality, in terms of the reciprocity, of the measured data.

The convergence history of the object function is shown in Fig. 6, and the convergence in the flow resistivity is illustrated in Fig. 7. For the fibrous glass wool tested, the identified flow resistivity tensor, in ($Pa\,s/m^2$), is shown in the following equation:[2]

$$\boldsymbol{\sigma} = \begin{bmatrix} 10\,800 & 34 & 28 \\ 34 & 6200 & 64 \\ 28 & 64 & 5800 \end{bmatrix} \ (Pa\,s/m^2) \tag{18}$$

The relative error in the pressure differences for the optimal solution, i.e. the components corresponding to Eq. (17), is given by the following equation:

$$\boldsymbol{\varepsilon}^{\text{glassfibre}} = \begin{bmatrix} -0.04 & -0.18 & -0.18 & -0.09 & 0.08 \\ 0.24 & 0.02 & 0.02 & 0.05 & -0.11 \\ 0.14 & -0.04 & 0.02 & -0.11 & 0.11 \end{bmatrix} \tag{19}$$

The largest differences occur for the cross flow directions, i.e., faces 6 to 1, faces 3 to 5 and faces 2 to 1. There are several sources contributing to this, e.g. glue residue used to hold a removed impermeable layer on the surface of the acoustic material, an in-homogeneity of the fibre organisation in the sample, etc. The main flow directions show, however, rather low errors.

The air flow inside the cubic test sample is illustrated in Fig. 8, where the pressure and the corresponding streamlines are shown for one in-flow (face 6), out-flow (face 1) combination. Note the curvature of the isosurfaces of the pressure along the face opposite the in-flow, for an isotropic material these would be plane.

[2] All numerical values presented for the flow resistivities throughout the paper are rounded off to three significant digits.

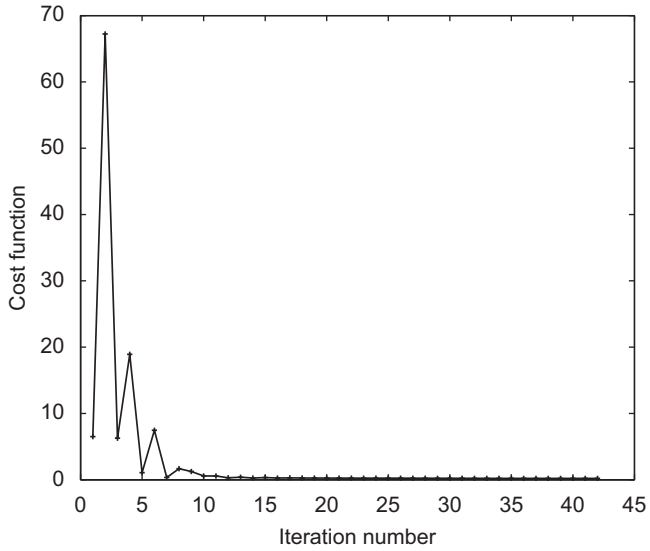

Fig. 6. Iteration history for fibrous glass wool sample, vertical axis shows cost function defined in Eq. (9).

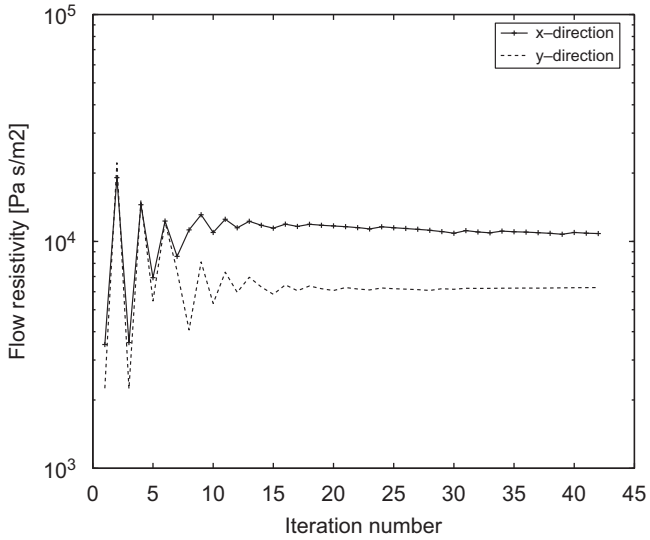

Fig. 7. Iteration history for fibrous glass wool sample for σ_{xx} and σ_{yy} in (Pa s/m^2).

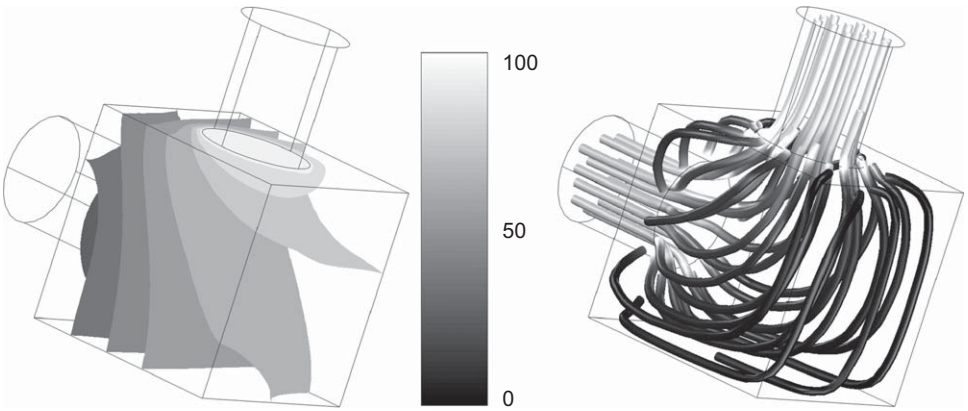

Fig. 8. Predicted pressure (left) and velocity (right) distribution for inflow at face 6 and outflow at face 1 for fibrous wool. Scale in percentage of the maximum value.

Table 2
Pressure differences (Pa) measured for porous foam sample.

	Face 1	Face 2	Face 3	Face 4	Face 5	Face 6
Face 1	–	313.7	363.4	281.4	317.7	300.8
Face 2	314.5	–	335.8	386.5	371.3	332.3
Face 3	365.0	337.6	–	321.8	339.8	331.2
Face 4	283.3	388.0	319.8	–	322.0	328.3
Face 5	316.5	368.6	336.5	320.0	–	400.8
Face 6	298.8	329.5	328.0	325.6	401.7	–

The identified data could also qualitatively be compared to the results published in the literature by Allard [5] and Tarnow [6]. Considering the diagonal elements of the flow resistivity tensor, it is deduced that the relation between the stacking direction, through the thickness, and the in plane, should be on the average $1{:}\frac{2}{3}$ for an ideal theoretical, transversely isotropic, wool, Tarnow [6], and about $1{:}\frac{1}{2}$ from measurements on a real material. Allard [5], found a ratio of 0.6 from acoustical measurements. The results shown above point to the ratio being 0.57, closer to the experimental findings of Tarnow [6] and Allard [5], rather than the theoretical d:o.

5.2. Application to porous foam

Following the successful verification of the inverse estimation procedure and the subsequent identification of the flow resistivities of a fibrous wool, a porous foam sample with density about 36 $\mathrm{kg/m^3}$, was also investigated. Due to a more complex micro-structural topology it could be expected that the degree of anisotropy would be considerably higher for such a material.

Following the preparatory steps outlined above, the measured pressure differences obtained are shown in Table 2, once again clearly exhibiting a close to symmetric, high quality data set.

Using the inverse estimation procedure discussed above, Eq. (9), and the measured pressure differences over the cubic foam sample, Table 2, the flow resistivity tensor matrix shown in Eq. (20) was found.

$$\boldsymbol{\sigma} = \begin{bmatrix} 12\,000 & 1570 & 1430 \\ 1570 & 14\,400 & 1380 \\ 1430 & 1380 & 13\,200 \end{bmatrix} \ (\mathrm{Pa\,s/m^2}) \tag{20}$$

The relative error in pressure differences in the optimal solution, i.e. the components corresponding to Eq. (17) for the porous foam, is given by Eq. (21). The largest differences occur also for the foam sample for the cross flow direction, i.e., faces 6 to 1. The main flow directions, in agreement to the glass wool results, exhibit rather small errors. Furthermore, it is also interesting to note that the error levels are quite similar in magnitude in the corresponding in-flow and out-flow combinations for the two types of materials, having fundamentally different micro-structural topology.

$$\boldsymbol{\varepsilon}^{\mathrm{foam}} = \begin{bmatrix} -0.01 & -0.005 & 0.02 & -0.07 & 0.08 \\ 0.14 & 0.008 & 0.06 & -0.01 & 0.006 \\ 0.04 & -0.07 & -0.01 & -0.10 & -0.04 \end{bmatrix} \tag{21}$$

6. Principal directions

The full anisotropic flow resistivity tensors determined using the inverse estimation procedure discussed above, obviously depends on the orientation of the samples tested and the inherent directivities induced by the manufacturing processes used. An alternative picture and perhaps also a better understanding of the intrinsic flow resistivity of the materials may be gained by computing the eigenvalues and eigenvectors of the flow resistivity matrices, i.e. through determination of the principal directions and their corresponding principal flow resistivities.

6.1. Fibrous wool

Starting from the identified tensor, Eq. (18), the principal directions for the flow resistivity of the investigated glass wool were identified in terms of its eigenvalues and eigenvectors. Solving the eigenvalue problem, three distinct principal flow resistivities, in units ($\mathrm{Pa\,s/m^2}$), are obtained

$$\begin{aligned} \sigma_1 &= 10\,800 \\ \sigma_2 &= 6300 \\ \sigma_3 &= 5800 \end{aligned} \tag{22}$$

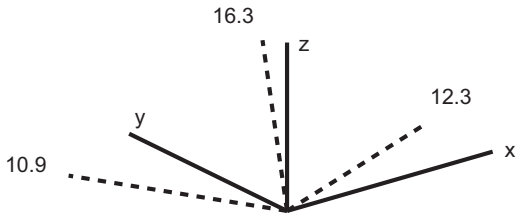

Fig. 9. Principal directions for original data shown together with body coordinate system. Indicated are also the flow resistivities in the principal directions in (10^3 Pa s/m^2).

together with three orthogonal, directional eigenvectors,[3]

$$\begin{aligned}\boldsymbol{\phi}_1 &= \{-1.00\ \ 0.00\ \ 0.00\}\\ \boldsymbol{\phi}_2 &= \{0.00\ \ 0.99\ \ -0.14\}\\ \boldsymbol{\phi}_3 &= \{0.00\ \ 0.14\ \ 0.99\}\end{aligned} \tag{23}$$

It was found that the estimated flow resistivity tensor is for all practical purposes transversely isotropic, see Eq. (22), the highest flow resistivity estimated in a direction parallel to the body coordinate axis through the thickness of the material, in this case the *x*-direction.

6.2. Porous foam

A similar analysis was performed for the polymer foam, i.e. the eigenvalues and eigenvectors of Eq. (20), were computed as three distinct principal flow resistivities in (Pa s/m^2),

$$\begin{aligned}\sigma_1 &= 10\,900\\ \sigma_2 &= 12\,300\\ \sigma_3 &= 16\,300\end{aligned} \tag{24}$$

and three orthogonal, directional eigenvectors

$$\boldsymbol{\phi}_1 = \{-0.88\ \ 0.24\ \ 0.41\}$$

$$\boldsymbol{\phi}_2 = \{0.18\ \ -0.64\ \ 0.74\}$$

$$\boldsymbol{\phi}_3 = \{0.44\ \ 0.73\ \ 0.52\} \tag{25}$$

Also for this particular material, it appears as if an assumption about transverse isotropy would be a reasonable approximation. A graphical representation of the principal directions is included in order to provide additional insight into the understanding of the flow resistivity properties of this foam, see Fig. 9.

7. Sensitivity in estimated flow resistivities due to errors in measured data

To get a first and preliminary view of the sensitivity in the estimated flow resistivities with respect to errors in the measured differential pressures, additional inverse estimations for two different cases were carried out. One case was focussed on the influence of errors in individual measured data and the other on the repeatability. Thus, as an example of the first kind of plausible errors, the flow resistivity tensor for the fibrous wool was re-estimated for artificially perturbed input data. To study the repeatability, the same foam sample was dismounted and re-mounted in the measurement device and the test was repeated.

7.1. Perturbation of flow combination with high error in estimation

This artificial modification of the measured data was introduced on the in-flow–out-flow combination exhibiting the largest error in the original estimation. For this purpose the measured pressure differences given in Table 1, were increased by 10 percent for in-flow at face 1–out-flow at face 6 and in-flow at face 6–out-flow at face 1. These in-flow–out-flow combinations exhibit the largest errors for both types of materials, see Eqs. (19) and (21), and it should be interesting to get an estimate of the sensitivity of the overall flow resistivity tensor in this respect.

Running the inverse estimation, i.e. solving Eq. (9), with data perturbed as discussed above, the flow resistivity matrix shown in Eq. (26) was found. As compared to the estimated flow resistivity determined for the original data set, Eq. (18),

[3] The eigenvalues and eigenvectors were in all cases throughout the paper computed using the full numerical precision in the flow resistivity tensor, thus a calculation based on the flow resistivity values given in the paper will deviate slightly.

the diagonal elements have changed, but to a lower extent than the actual perturbation introduced. The off-diagonal elements corresponding to the flow directions for these faces were increased, but they remain significantly lower than the diagonal.

$$\boldsymbol{\sigma} = \begin{bmatrix} 11\,600 & 500 & 300 \\ 500 & 5800 & 62 \\ 300 & 62 & 5800 \end{bmatrix} \ (\mathrm{Pa\,s/m^2}) \tag{26}$$

Computing the eigenvalues and eigenvectors of the matrix given in Eq. (26), results in the estimated flow resistivities for the glass wool shown in Eq. (27) in ($\mathrm{Pa\,s/m^2}$). Also for the principal values, the variation in the flow resistivities appears to be lower than the actual error introduced and the principal directions remain essentially the same.

$$\begin{aligned} \sigma_1 &= 11\,700 \\ \sigma_2 &= 5800 \\ \sigma_3 &= 5900 \end{aligned} \tag{27}$$

7.2. Repeated test for foam sample

The foam sample previously tested, was re-mounted in the measurement device and the pressure differences were recorded again, see Table 3. A direct comparison between the two sets of data, gives the relative errors shown in Table 4. The highest error is less than 6 percent.

Feeding the values shown in Table 3 into the estimation procedure resulted in the estimated flow resistivity matrix shown in Eq. (28). It is interesting to note that the largest difference in the estimated flow resistivities, σ_{yz}, do not correspond to the cross-flow directions with the largest relative error, i.e., x–z.

$$\boldsymbol{\sigma} = \begin{bmatrix} 12\,800 & 1700 & 1800 \\ 1700 & 13\,800 & 460 \\ 1800 & 460 & 13\,500 \end{bmatrix} \ (\mathrm{Pa\,s/m^2}) \tag{28}$$

To get further insight into the repeatability and to analyse the variations in the estimated data in relation to the subsequent flow resistivity estimates, the three distinct principal flow resistivities in ($\mathrm{Pa\,s/m^2}$), were also computed for the repeated test data set,

$$\begin{aligned} \sigma_1 &= 10\,800 \\ \sigma_2 &= 13\,200 \\ \sigma_3 &= 16\,000 \end{aligned} \tag{29}$$

Table 3
Pressure differences (Pa) measured in repeated test of porous foam sample.

	Face 1	Face 2	Face 3	Face 4	Face 5	Face 6
Face 1	–	324.9	379.4	294.4	327.4	300.5
Face 2	321.9	–	354.0	396.7	379.4	333.0
Face 3	379.6	354.4	–	327.4	350.2	334.8
Face 4	292.5	396.3	324.7	–	327.1	327.1
Face 5	327.2	378.4	348.5	324.7	–	401.2
Face 6	302.4	332.1	335.2	326.6	400.6	–

Table 4
Absolute relative errors in (percent) for recorded pressure differences for repeated tests of porous foam sample.

	Face 1	Face 2	Face 3	Face 4	Face 5	Face 6
Face 1	–	3.6	4.4	4.6	3.1	0.1
Face 2	2.4	–	5.4	2.6	2.2	0.2
Face 3	4.0	5.0	–	2.6	2.2	0.2
Face 4	3.2	2.1	1.6	–	1.6	0.4
Face 5	3.4	2.7	3.6	1.5	–	0.1
Face 6	1.2	0.1	2.2	0.3	0.3	–

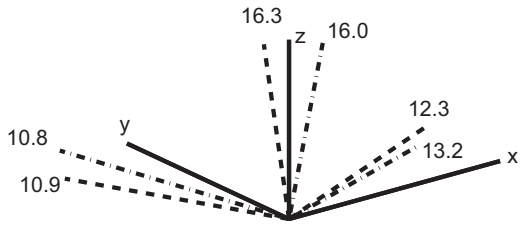

Fig. 10. Principal directions for original data, dotted line, and for data from repeated measurement on same foam sample, dash–dotted. Indicated are also the flow resistivities in the principal directions in (10^3 Pa s/m^2).

Table 5
Computed flow resistivities according to Eq. (31) and measured flow resistivities in (Pa s/m^2) for a cylindrical sample of glass wool in different body coordinate directions.

Coordinate direction	Computation using Eq. (18)	Measurement
x	10 800	11 000
y	6200	–
z	5900	–

with three orthogonal, directional eigenvectors

$$\boldsymbol{\phi}_1 = \{-0.79 \;\; 0.38 \;\; 0.48\}$$

$$\boldsymbol{\phi}_2 = \{0.07 \;\; -0.72 \;\; 0.69\}$$

$$\boldsymbol{\phi}_3 = \{0.61 \;\; 0.58 \;\; 0.54\} \tag{30}$$

The flow resistivity in the second principal direction, having its largest component in the y-direction, shows the largest change, about 7 percent. However, in the direction of the highest flow resistivity, the values found are practically the same. This is also confirmed by a study of the principal directions in a graphical representation, see Fig. 10.

8. Validation of identified anisotropic flow resistivity

To validate the estimated anisotropic flow resistivity obtained for the tested materials, cylindrical specimens applicable in the standard measurement set up were extracted from the tested glass wool cubic sample. Due to the thickness of the available tested material, only one cylindrical sample was possible to extract in the body coordinate direction x, and the resulting flow resistivities are given in the second column of Table 5.

In general, to validate the estimated flow resistivity tensor, samples would need to be extracted in the principal directions and then measured in the standard set-up. This is straightforward for the fibrous wool, but more complicated for a porous foam. An alternative approach would be to simulate the standard test set-up using the estimated flow resistivity tensor. The argument is that if this is a true property of a material tested, then it should also be able to reproduce the pressure difference measured in a standard test set up using cylindrical samples. Thus, in order to validate the estimated flow resistivity tensor given by Eq. (18), a new set of simulations were performed for a cylindrical tube geometry and the results evaluated according to Eq. (31) . The outcome of these simulations are given for the glass wool in the first column of Table 5.

$$\sigma^{cyl} = \frac{\Delta p}{LV} \tag{31}$$

The agreement for the glass wool is remarkable and constitute a first validation of the anisotropic estimation procedure discussed here. Further support for the validity may be found in Ref. [6], Fig. 2, where data for a glass wool with similar density, measured in the directions parallel to the fibres lie close to the values estimated here.

9. Conclusions

With the proposed novel method the full, anisotropic flow resistivity tensors of samples of a fibrous wool and a foamed polymer have been identified. Computing the eigenvalues and eigenvectors of the estimated tensors it was found that the respective flow resistivity tensor is transversely isotropic for the tested glass wool and close to transversely isotropic for the tested foam. This latter result is to our knowledge new. For the fibrous wool the principal directions are aligned with

the material layers, the estimated values agree with a static flow resistivity from standard measurement and the estimated flow resistivity qualitatively matches published data for glass wool.

The repeatability, and the corresponding variation in the estimated flow resistivities, of the proposed approach appears to be satisfactory. Repeated tests on a foam sample indicated a variation in measured pressure differences of around 5 percent in any cross-flow combination. The largest variation in the estimated flow resistivities is then around 7 percent, but the principal directions are slightly rotated. These differences appear moderate, but the actual impact in terms of simulated foam behaviour in a practical application situation has to be investigated before a more general conclusion can be drawn.

From the results discussed in the present paper, it appears as if the estimation approach used is robust to errors in the input data, in the sense that they change in proportion to the perturbations introduced. This was demonstrated through different estimations on varied data sets. However, to generalise this conclusion a more thorough investigation would be required, in particular involving materials with a higher degree of anisotropy than the two different types discussed here.

Obviously the validity of the estimated flow resistivity is not only dependent on the measurement data, but also the numerical accuracy in the solution is an important aspect. To assure converged solutions of the Darcy flow problem in each realisation and at the same time keeping the computational effort at a manageable level, adaptation of meshes for optimal convergence is a crucial step. Furthermore, different meshing strategies could be used for different in-flow out-flow combinations, the choices being guided by the errors between estimated and measured pressure differences as reflected by Eq. (17).

Acknowledgements

The authors would like to acknowledge the support from the European Union, the Friendcopter project (Contract no. AIP3-CT-2003-502773) under which parts of the research has been performed. The authors would also like to express their appreciation to Mr Kent Lindgren and Mr Danilo Prevelić for their precious help with the set up and the experiments.

Appendix A. Positive definiteness of flow resistivity tensor

The estimation of the flow resistivity tensor must lead to positive definiteness. To ensure this, side conditions and bounds were used in the inverse problem, see Eqs. (11)–(13). In this Appendix these relations are derived as follows.

The flow resistivity tensor, assuming symmetry and that all diagonal terms are positive and non-zero, is given by

$$\boldsymbol{\sigma} = \begin{bmatrix} \sigma_{11} & \sigma_{12} & \sigma_{13} \\ \sigma_{12} & \sigma_{22} & \sigma_{23} \\ \sigma_{13} & \sigma_{23} & \sigma_{33} \end{bmatrix} \tag{A.1}$$

if this tensor is positive definite, then its determinant must be a non-zero and positive number. Calculating the determinant leads to

$$\sigma_{11}\sigma_{22}\sigma_{33} + 2\sigma_{12}\sigma_{13}\sigma_{23} - \sigma_{13}^2\sigma_{22} - \sigma_{23}^2\sigma_{11} - \sigma_{12}^2\sigma_{33} > 0 \tag{A.2}$$

which may be rearranged as

$$\frac{\sigma_{23}^2}{\sigma_{22}\sigma_{33}} + \frac{\sigma_{13}^2}{\sigma_{11}\sigma_{33}} + \frac{\sigma_{12}^2}{\sigma_{11}\sigma_{22}} - 2\frac{\sigma_{12}\sigma_{13}\sigma_{23}}{\sigma_{11}\sigma_{22}\sigma_{33}} < 1 \tag{A.3}$$

Since also the inverse of the flow resistivity tensor, i.e., the permeability tensor, must be positive definite, it follows that the diagonal terms of the inverse must also be positive and non-zero. These are given by the minors of the flow resistivity tensor, here exemplified by the 11-element as

$$\kappa_{11} = \frac{\sigma_{22}\sigma_{33} - \sigma_{23}^2}{|\boldsymbol{\sigma}|} > 0 \tag{A.4}$$

which leads to the following condition on the terms of the flow resistivity tensor:

$$\frac{\sigma_{23}^2}{\sigma_{22}\sigma_{33}} - 1 < 0 \tag{A.5}$$

Similarly the other minors be derived and the three first terms of Eq. (A.3), may be identified as the corresponding to the minors, 11, 22 and 33 respectively.

References

[1] H. Darcy, *Fontaines publiques de la ville de dijon*, Libraire des Corps. Impériaux des Ponts et Chaussées et des Mines, Paris, 1856.
[2] M.A. Biot, Theory of propagation of elastic waves in a fluid-saturated porous solid. I. Low frequency range, *Journal of the Acoustical Society of America* 28 (1956) 168–178.

[3] D.L. Johnson, J. Koplik, R. Dashen, Theory of dynamic permeability and tortuosity in fluid-saturated porous media, *Journal of Fluid Mechanics* 176 (1987) 379–402.
[4] J.F. Allard, *Propagation of sound in porous media: modelling sound absorbing materials*, Elsevier Applied Science, 1993 (0-387-98319-8).
[5] J.F. Allard, R. Bourdier, A. L'Esperance, Anisotropic effect in glass wool on normal impedance in oblique incidence, *Journal of Sound and Vibration* 114 (1987) 233–238.
[6] V. Tarnow, Measured anisotropic air flow resistivity and sound attenuation of glass wool, *The Journal of the Acoustical Society of America* 111 (2002) 2735–2739.
[7] J. Tran-Van, X. Olny, *Acoustic and elastic parameters determination for anisotropic mineral wools*, Acta Acustica United With Acustica S20 (2005).
[8] M.D. Sharma, Wave propagation in a general anisotropic poroelastic medium with anisotropic permeability: phase velocity and attenuation, *International Journal of Solids and Structures* 41 (16–17) (2004) 4587–4597.
[9] S.S. Kohles, et al., Direct perfusion measurements of cancellous bone anisotropic permeability, *Journal of Biomechanics* 34 (2001) 1197–1202.
[10] J. Tran-Van, Etude de l'influence de l'isotropie tranverse des laines minerales sur la transmission acoustique des parois multicouches—study on the influence of anisotropy on mineral wool for acoustical transmission on multi layered medium, PhD Thesis, Ecole supérieure d'ingénieurs de Poitiers, 2004.
[11] International Organization for Standardization, Geneva, Switzerland, *Iso 9053:1991: acoustics—material for acoustical application—determination of airflow resistance*, 1991.
[12] J.-F. Despois, A. Mortensen, Permeability of open-pore microcellular materials, *Acta Materialia* 53 (5) (2004) 1381–1388.
[13] L. Wang, Flows through porous media: a theoretical development at macroscale, *Transport in Porous Media* 39 (2000) 1–24.
[14] M.A. Biot, Mechanics of deformation and acoustic propagation in porous media, *Journal of Applied Physics* 33 (1962) 1482–1498.
[15] Comsol multiphysics 3.4, Last view: March 2008 ⟨www.comsol.com⟩.
[16] K. Svanberg, Method of moving asymptotes—a new method for structural optimization, *International Journal for Numerical Methods in Engineering* 24 (1987) 359–373.